



# Sorption and separation performance of certain natural radionuclides of environmental interest using silica/olive pomace nanocomposites

G. A. Dakroury<sup>1</sup> · K. F. Allan<sup>1</sup> · M. F. Attallah<sup>2</sup> · E. M. El Affi<sup>2</sup>

Received: 15 April 2020 / Published online: 6 June 2020  
© Akadémiai Kiadó, Budapest, Hungary 2020

## Abstract

This study is concerned with the sorption behavior of natural radionuclides ( $^{226}\text{Ra}$ ,  $^{210}\text{Po}$ ,  $^{228}\text{Th}$ —originated from TENORM waste associated with petroleum industry) onto silica/olive pomace nanocomposite. Initially, nanocomposites of extracted silica and olive pomace are prepared and characterized by physicochemical techniques. In the batch technique, 60%  $\text{SiO}_2$  40% olive pomace (AM3) nanocomposite showed a considerable group sorption for  $^{226}\text{Ra}$  and  $^{210}\text{Po}$  larger than  $^{228}\text{Th}$  in 1M  $\text{HNO}_3$  and  $\text{HClO}_4$  solutions. In case of sorption by the compacted disc, sorption of  $^{226}\text{Ra}$  was similar to batch method, sorption of  $^{228}\text{Th}$  increased slightly to ~17%, while sorption of  $^{210}\text{Po}$  was decreased to 77%. Thus, AM3 nanocomposite can be considered as an efficient nano-adsorbent for sorption and separation of Ra-isotopes and  $^{210}\text{Po}$ -radionuclides from  $^{226}\text{Ra}$ – $^{210}\text{Po}$ – $^{228}\text{Th}$  admixture associated with nuclear and non-nuclear industries.

**Keywords** Nanomaterial · Biomass waste · Sorption · Separation · Radionuclides ( $^{226}\text{Ra}$ ,  $^{210}\text{Po}$ ,  $^{228}\text{Th}$ )

## Introduction

The nanocomposite materials are extensively prepared and developed using various inorganic metal oxides and organic gradients [1]. Nowadays, these materials have been used in a number of technological fields of the industrial and/or nuclear interest [2]. Thus, the nanomaterials can be used in many applications such as thin-film capacitors for computer chips, solid polymer electrolytes for batteries, automotive engine parts and fuel tanks and/or waste management [3].

Utilization of plant biomass to produce engineering materials attracted the attention of scientists to encompass the technological of scientific aspects such as economic, industrial, and environmental cases [4]. Rice husk and rice husk ash are interesting sources of considerable levels of high quality silica [5]. Olive pomace consists of a ligno-cellulosic matrix with polyphenolic compounds, uronic acids, and oily residues [6]. Numerous sites, potentially active in

metal removal, such as carboxylic, hydroxyl, methoxy, and phenolic groups are present. Polysaccharides as starch gel have been used as a template to obtain macroporous material and film [7, 8].

The TENORM wastes are defined as, naturally occurring radioactive materials that have been concentrated or exposed to the accessible environment as a result of human activities such as manufacturing, mineral extraction, water processing, non-nuclear industries such as phosphate reprocessing, and petroleum industries have contained natural radionuclides of uranium and thorium series. These have decayed daughters of Ra, Rn, Th, Po, Pb radionuclides [9, 10]. All these applications generate radioactive waste that may represent risks to the environment or to human beings, but it is necessary to have special attention to the management of these radioactive wastes [11, 12].

Recently, different of technologies have been studied as potential means of attenuating radionuclide concentration, such as precipitation, membrane filtration, sorption, ion exchange, etc. [13–16]. Among these methods, the adsorption methods have been widely utilized because it is easily achieved, economical and can be applied on a large scale for practical applications. Some adsorbent nanomaterials, such as clay minerals [17–22] and inorganic oxides [23–27] have been investigated extremely for the treatment the effluents containing the radionuclides of environmental

✉ G. A. Dakroury  
dr\_gdakroury2010@yahoo.com

<sup>1</sup> Nuclear Chemistry Department, Hot Laboratories Centre, Atomic Energy Authority, Cairo 13759, Egypt

<sup>2</sup> Analytical Chemistry and Control Department, Hot Laboratories Center, Atomic Energy Authority, Cairo 13759, Egypt

and/or nuclear interest. However, these effluents containing an enhanced activity levels than the permitted safe limits [28–30].

Herein, the authors concerned with the development of novel nanomaterials/nanocomposites with low cost, sufficient surface functional groups and high sorption ability for the separation trace level of some natural radionuclides ( $^{226}\text{Ra}$ ,  $^{210}\text{Po}$ ,  $^{228}\text{Th}$ ) of environmental and human health concern. Thus, this work aims to prepare silica/olive pomace nanocomposite by wet chemical technique. Different ratios of olive pomace, as an agricultural waste, added to silica, extracted from Egyptian rice husk. The prepared nanocomposite powders were characterized by physic-chemical techniques as SEM, EDX, TEM, XRD, DTA–TGA, FTIR, pore-size analysis and BET surface area. The dried prepared samples were pressed using the dry press method at a pressure 8000 psi to get compact disc. Sorption behavior of the dried powders and the compact disc towards  $^{226}\text{Ra}$ ,  $^{210}\text{Po}$  and  $^{228}\text{Th}$  as trace natural radioactive waste from the TENORM-concentrate was studied. Optimization of the olive–Pomace ratio and the acid solution for  $^{226}\text{Ra}$ ,  $^{210}\text{Po}$  and  $^{228}\text{Th}$  separation were also investigated.

## Experimental

### Chemicals and reagents

The rice husk (RH) was collected from Egyptian fields as agricultural waste to prepare the silica nanoparticles, Olive pomace from South Sinai, HCl and NaOH purchased from (Edwak, Egypt). The samples were ground in the mill and then sieved to 75  $\mu\text{m}$ . TENORM-concentrate was provided from treatment of the scale wastes associated with petroleum and natural gas exploration. Barium chloride ( $\text{BaCl}_2$ ),  $\text{PbCl}_2$ , HF,  $\text{H}_3\text{BO}_3$ ,  $\text{HClO}_4$ , and  $\text{HNO}_3$  purchased from Sigma-Aldrich Co, USA. Double distilled water (DDW) was used in all experiments. All the reagents used in this study were analytical grade (AR Grade) and used as received without further purification.

### Extraction of nano-silica from Egyptian rice husk

The pure nano-silica powder was extracted from Egyptian Rice husk by controlling different process parameters. The obtained rice husk was washed thoroughly with distilled water to remove any adhering impurities. The washed rice husk was dried at 80  $^\circ\text{C}$  and then burnt at 800  $^\circ\text{C}$  for 2 h in a muffle furnace. The carbonized rice husk was refluxed with 1M HCl for 2 h and then filtered to remove metallic impurities and to extract pure nano-silica. The filtered was thoroughly washed with DDW till pH 6 and then dried at 105  $^\circ\text{C}$  for a day. The dried sample was burned in a muffle

at 800  $^\circ\text{C}$ /1 h with heating rate 10  $^\circ\text{C}/\text{min}$  then cooled to environment temperature. Finally, the obtained silica was boiled with 1M NaOH at 100  $^\circ\text{C}$ /1 h with constant stirring. After cooling, samples was filtrated and titrated with 1M HCl then soaked in the same solution for 48 h. Then the resulting silica was washed with distilled water and centrifuge to separate solid from solution for removing free Na and Cl. The separated silica was dried at 100  $^\circ\text{C}$ /48 h [28]. The weight percent of Si in the extracted silica was ~50%.

### Preparation of silica/olive pomace nanocomposite materials (Group A)

20% and 30% and 40% of olive pomace were added to extracted silica in order to prepare different nanocomposites compositions of silica-olive pomace. The nanocomposites were prepared using wet-chemical technique. The extracted silica was dissolved in alcoholic solution of ethanol and the mixture is acidified with 1M HCl. The obtained mixture was stirred using the magnetic stirrer for 30 min. Different ratios of pomace olive added gradually with vigorous stirring. The mixture was laid in ultrasonic instrument for 10 min. The whole mixture was stirred for 24 h before drying at 60  $^\circ\text{C}$  for 48 h. The dried powders were used in batch sorption studies and labeled group A (M1–M3) as illustrated in Table 1.

### Preparation of silica-olive pomace/starch nanocomposite materials (Group B, C)

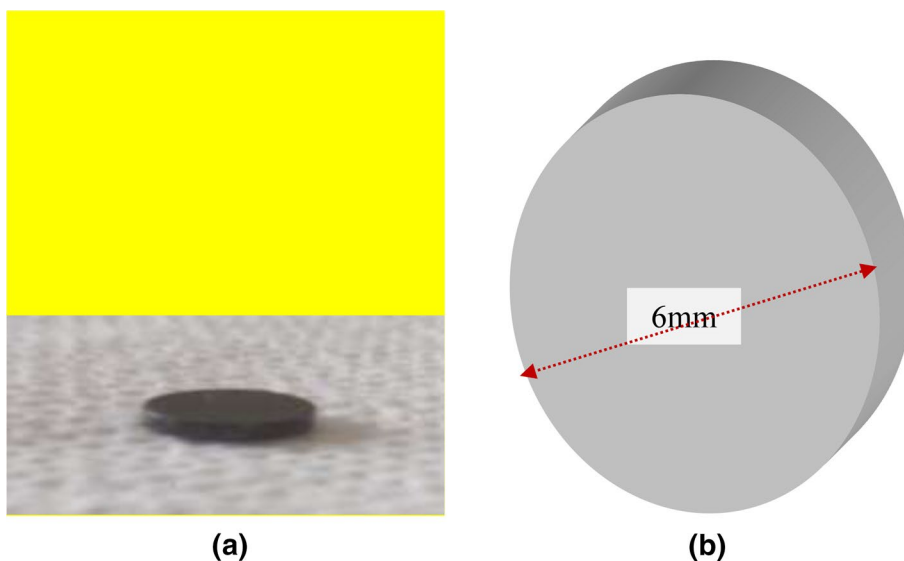
Soluble starch (30 g) was dissolved in 100 mL hot distilled water. 1.0, 1.5 and 2.0 g of olive pomace and 4 g, 3.5 g, and 3 g of extracted silica were added in order to prepare three different nanocomposites compositions (20, 30 and 40% respectively) of silica/olive pomace. The mixtures were heated at 90–100  $^\circ\text{C}$  and magnetically stirred till the mixed solution gradually became highly viscous. The gel solution was maintained at that temperature for 180 min, after which it was cooled to room temperature and left at 4  $^\circ\text{C}$  for 48 h (solution-phase stage). Then the solvent was replaced with ethanol and the “solid” formed was separated from the mother solution by decantation method. The solid was dried at 80  $^\circ\text{C}$  for overnight, labeled Group B (M4–M6). The dried powder were calcined at 600  $^\circ\text{C}$  for 2 h in an air atmosphere [31] Labeled Group C(M7–M9). Table 1 includes the chemical compositions and sample codes for the prepared sample groups.

### Fabrication of compact disc

The dried prepared samples were pressed using the dry press method at a pressure 8000 psi to get compact disc. The raw samples put into die cavities with the addition of 1–2 wt% of polyvinyl alcohol. A strong compact discs were fabricated

**Table 1** The chemical compositions and samples codes for the prepared sample groups

Group	Material code	Composition materials	Drying temperature (°C)
A	AM1	80% SiO <sub>2</sub> + 20% olive pomace	60 °C
	AM2	70% SiO <sub>2</sub> + 30% olive pomace	
	AM3	60% SiO <sub>2</sub> + 40% olive pomace	
B	BM4	80% SiO <sub>2</sub> + 20% olive pomace in 30% starch solution	60 °C
	BM5	70% SiO <sub>2</sub> + 30% olive pomace in 30% starch solution.	
	BM6	60% SiO <sub>2</sub> + 40% olive pomace in 30% starch solution.	
C	CM7	80% SiO <sub>2</sub> + 20% olive pomace in 30% starch solution.	600 °C
	CM8	70% SiO <sub>2</sub> + 30% olive pomace in 30% starch solution.	
	CM9	60% SiO <sub>2</sub> + 40% olive pomace in 30% starch solution.	

**Fig. 1** Pictures for compacted disc (a real disc, b structural disc diameter)

and used in sorption studies by filtration system. An amount of 85 mg of the prepared samples was efficiently compacted with thickness ( $l$ ) of 2 mm and diameter ( $\phi$ ) of 6 mm, Fig. 1. Then, the prepared compacted disc was assembled for use in a vacuumed filtration unit as seen in Fig. 2.

### Preparation of radionuclides source

In this study, we explored three natural radionuclides ( $\alpha$ -emitters, <sup>226</sup>Ra, <sup>210</sup>Po and <sup>228</sup>Th) of environmental interest from the TENORM-concentrate. The radionuclides include Ra-isotopes as <sup>226</sup>Ra, <sup>228</sup>Ra (source for <sup>228</sup>Th) and <sup>210</sup>Pb (source for <sup>210</sup>Po). The collected TENORM-concentrated as reported in our previous study [32] which was used as a source of these radionuclides. However, the source of this concentrate was extracted from the TENORM scale waste associated with petroleum exploration in Ras-Shukeir oil-field (coordinates: 28.131414° N, 33.248477° E), area of the Gulf of Suez, North of Hurghada (Red Sea Governorate),

**Fig. 2** Filtration unit used for separation by compact disc technique

Egypt. Initially, the waste concentrate was dried, crushed, grounded and sieved to grain sizes below 0.1 mm. About 2 g of the sample is weighed in 250-cm<sup>3</sup> Teflon beaker. Moreover, 50 mg of Ba<sup>2+</sup> and Pb<sup>2+</sup> are added to the sample before digestion, as carrier with moistening using DDW. Then, digestion of the sample is carried as described by elsewhere [33, 34] with some modifications. Inside fume hood, the sample was cooked by open digestion procedure using sand bath within temperature 80–100 °C. The sample was digested by successive additions of HF (32%), H<sub>3</sub>BO<sub>3</sub> + DDW, aqua regia (HClO<sub>4</sub> and HNO<sub>3</sub>). Appearance of colorless paste indicates to ending of the sample digestion. The sample is dissolved quantitatively by 2.5 ml Conc. HNO<sub>3</sub> and transferred into polyethylene (PE) tube (50-cm<sup>3</sup>), then, the solution completed by DDW till 25 ml. The obtained turbid solution was centrifuged. Then, the clear stock solution was separated by decantation into PE-tube. Radiometric measurements for all  $\gamma$ -emitters in sample solution by gamma ray spectrometer are done to evaluate the digestion efficiency and the stock solution. It was found that the efficiency of the modified digestion procedure was > 95%. On the other hand, the stock solution had been examined by an alpha-spectrometer to identify and confirming the presence of <sup>226</sup>Ra, <sup>210</sup>Po and <sup>228</sup>Th radionuclides in the stock solution.

## Instruments

An ultrasonic Cole-Parmer instrument (version hill, Illinois 60061, USA), was used in composites preparation. Fourier transform infrared (FT-IR), spectra were determined using a (Bomen Miclson FT-IR spectrophotometer, model MB157, Canada). The crystalline structure was studied using Shimadzu X-ray diffraction (XRD), (model XD-D1, Kyoto, Japan), with a diffraction angle (2 $\theta$ ) range of 4°–70°. Thermal analysis, DTA–TGA (system of type DTA–TGA-50, Japan), was used to study the phase changes and weight losses of the powder, respectively, at a constant rate of 5 °C/min from room temperature to 650 °C. The surface morphology of the prepared composites was investigated using scanning electron microscope (JEOL JSM-5400, Japan), and the nanostructure of the composite is investigated by transmission electron microscope (TEM), (JEM2100, Joel.s.b, Japan). The particle size of the prepared samples was determined using Zetasizer Nano-Zs, MALVERN, UK). Pore size distribution and corresponding porosity of the prepared samples were investigated using mercury intrusion porosimetry technique with the aid of (Pore-sizer chromatech 9320, USA).

The radiochemical recovery (%) of the modified digestion procedure used was estimated by measuring all  $\gamma$ -emitters in the TENORM concentrate before and after digestion within the same energy range (25–2620 keV). The measurements

were performed using a high purity germanium detector (detector type HPGe, model GX1020-10863, LN2 monitor, operating voltage of +3500 V, and resolution of 2 keV FWHM at 1332.5 keV peak of <sup>60</sup>Co, Geine-2000 software) provided from Canberra Industries Inc, USA. On the other hand, the net count rate (cps) of the studied alpha-emitters (<sup>226</sup>Ra, <sup>210</sup>Po and <sup>228</sup>Th) was assessed using an Integrated Alpha-Spectrometry System (model A65-B32, Version 5.10, Maestro-32 software) provided from EG&G ORTEC Instruments Inc., Oak Ridge, Tennessee, USA. The system contains eight chambers equipped by implemented silicon passivated detractors with operated at bias of positive voltage of 50 volts and resolutions  $\leq$  35 keV.

## Sorption studies

Nano-composites (AM1–CM9) had been examined towards removal some radionuclides of the environmental interest in the TENORM-concentrate solution. The attention herein was directed for removal of <sup>228</sup>Th, <sup>226</sup>Ra and <sup>210</sup>Po radionuclides. Initially, the sorption efficiency of the samples was carried out by the batch technique. However, 10 mL of the radionuclides mixture in nitric acid solution was shaken for equilibration with 0.05 g of the tested nanomaterial in polyethylene tubes (25-cm<sup>3</sup>) at room temperature (25  $\pm$  2 °C) for one day. The mixture was centrifuged at 4000 rpm for 15 min to separate the liquid from the tested samples. The clear liquor was separated by decantation to another pre-cleaned PE-tube. An accurate 50  $\mu$ L of the solution was spotted onto center of rounded stainless steel disc ( $\phi$  = 12 mm). Then, the disc was exposed to infrared light for drying the spotted sample solution. After cooling at room temperature, the disc was counted by an alpha spectrometer for at least 20,000 s. The uptake (%), distribution coefficient (K<sub>d</sub>, mL/g) and separation factors (SF) are calculated to evaluate the separation affinity of the prepared nano-composites towards the radionuclides admixture in the TENORM-concentrate using the next formulas [35]:

$$A (\%) = \left( \frac{C_i - C_f}{C_i} \right) \times 100 \quad (1)$$

$$K_d (\text{ml/g}) = \left( \frac{C_i - C_f}{C_f} \right) \times \frac{V}{m} \quad (2)$$

$$SF_{\frac{A}{B}} = \frac{K_d(A)}{K_d(B)} \quad (3)$$

where C<sub>i</sub> denotes to the net count rate of radionuclide before equilibration with the tested nanocomposites (AM1–CM9), C<sub>f</sub> refers to the net count rate of radionuclide after equilibration with the nanocomposite, V is the solution volume

of radionuclides mixed with the solid material and  $M$  is the mass of the nanocomposite used. In case of the ‘compact disc’ the sorption behavior for separation of the radionuclides was performed using vacuumed filtration unit as seen in Fig. 2. The results are the average of triplicate independent three measurements. The statistical errors in the radioactive measurements in uptake,  $K_d$  and SF calculations are  $< 5\%$ .

## Speciation diagram

The possible speciation diagram for the chemical behavior of radionuclides (especially  $^{226}\text{Ra}^{2+}$  and  $^{228}\text{Th}^{4+}$ ) in the different acid solutions was constructed using HYDRA\_MEDUSA software [36]. However, the database for the last version-2015 of this program does not contain speciation of the tetravalent polonium ( $\text{Po}^{+4}$  or  $\text{PoO}^{2+}$ ) used in this study. Thus, discussion and construction for speciation of Po(IV) in different acid solutions was achieved using some of those reported by elsewhere (cited in results and discussion, “Influence of acid solution type” section).

## Results and discussion

### Characterizations of nanocomposite

#### FT-IR analysis

FT-IR spectra were studied to distinguish various molecular vibrations that may exist in the crystal lattice of the prepared samples. Figure 3a–c are for extracted silica, olive pomace, and AM3, respectively. The peaks at 459, 621, and 789  $\text{cm}^{-1}$ , in Fig. 3a, indicates Si–O–Si bending, Si–H, and asymmetric Si–O–Si stretching modes of vibration, respectively [28, 37].

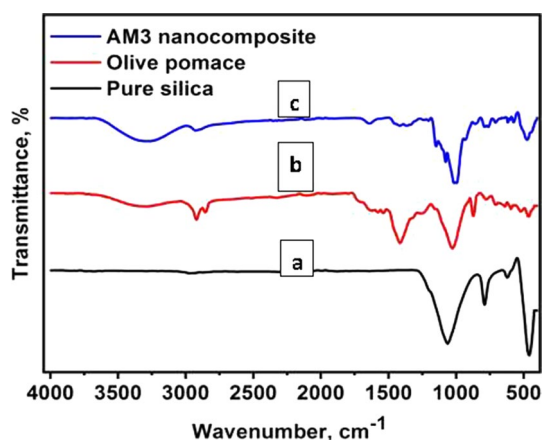


**Fig. 3** The FTIR spectra of **a** extracted silica, **b** olive pomace, **c** AM3 nanocomposite

The strong peak at 1062.84  $\text{cm}^{-1}$  is corresponding to Si–O stretching mode [38]. The weak band at 3863  $\text{cm}^{-1}$  assigned to remaining absorbed water while the peaks from 1281 to 2428  $\text{cm}^{-1}$  are because of residual impurities. Figure 3b shows an olive pomace pattern. Olive pomace is composed mainly of Cellulose, hemicelluloses, lignin, Carbohydrates, lipids, phenols and residual inorganic [39]. The peak at 3290  $\text{cm}^{-1}$  corresponding to hydrogen bonded –OH group (from carboxyls, phenols or alcohols) while the peaks at 2920 and 2854  $\text{cm}^{-1}$  assigned to asymmetric and symmetric stretching vibration of (cis) methylene group =CH, C–H group. The strong peak at 1439  $\text{cm}^{-1}$  related to carboxylate  $\text{COO}^-$  ion while the peak at 1027  $\text{cm}^{-1}$  due to connections of strain C–OH primary alcohol and CN. The broad absorption band between 1200 and 935  $\text{cm}^{-1}$  is attributed to the contribution of various functional groups, such as C–O and C–O–C [40]. The peak at 459  $\text{cm}^{-1}$  corresponds to Si–O–Si bond confirmed from EDX results. After Adding olive pomace to extracted silica, AM3, in Fig. 3c, carboxylate  $\text{COO}^-$  band at 1439  $\text{cm}^{-1}$  is disappeared. The broadness of OH peak at 3290  $\text{cm}^{-1}$  increases due to preparation technique while the 464  $\text{cm}^{-1}$  band intensity for Si–O–Si bending peak decreased due to decrease percentage of  $\text{SiO}_2$  (60%).

#### XRD analysis

Figure 4 shows the diffractograms of the extracted silica, Olive pomace and AM3 nanocomposite. Figure 4a, represent a crystalline structure as several studies have used different time and temperature conditions to produce amorphous or crystalline silica. However, most authors agree that amorphous silica is produced at temperatures below 800  $^{\circ}\text{C}$  [41]. The extracted silica from rice husk clarified crystalline phase form silica [5]. A sharp and strongest peak at  $2\theta$  value 21.7 ( $d = 4.07 \text{ \AA}$ ), and the other peaks at 20.7 ( $d = 4.287 \text{ \AA}$ ),

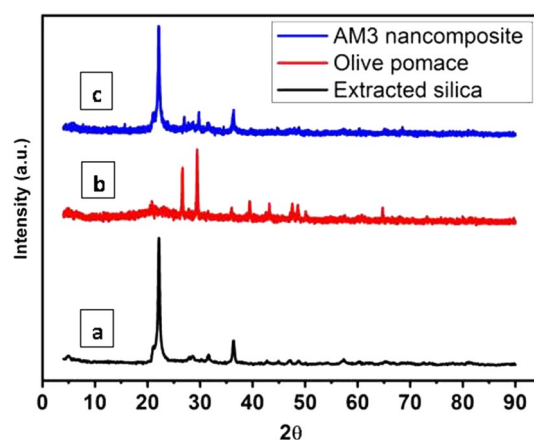


**Fig. 4** The XRD patterns of **a** extracted silica, **b** olive Pomace, **c** AM3 nanocomposite

27.63 ( $d=3.22 \text{ \AA}$ ), 31.26 ( $d=2.85 \text{ \AA}$ ), 35.99 ( $d=4.287 \text{ \AA}$ ). The International Centre for Diffraction Data database [42] reports tridymite ( $d=4.06 \text{ \AA}$ ,  $d=3.33 \text{ \AA}$ , and  $d=10.9 \text{ \AA}$ ), quartz ( $d=4.26 \text{ \AA}$  and  $d=3.34 \text{ \AA}$ ) and cristobalite ( $d=4.04 \text{ \AA}$ ,  $d=2.49 \text{ \AA}$ , and  $d=2.84 \text{ \AA}$ ) reflections [28]. While in Fig. 4b, the crystalline structure of the olive pomace mill at the peaks at  $2\theta$  value 29.42 ( $d=3.03 \text{ \AA}$ ), 26.62 ( $d=3.34 \text{ \AA}$ ) and 39.41 ( $d=2.26 \text{ \AA}$ ) is attributed to native cellulose while the other constituents of olive pomace are predominantly amorphous which is explained by the appearance of the spectrum [40]. For AM3, in Fig. 4c, the broad diffraction peaks nearly typical to those obtained from the extracted silica (at  $2\theta=21^\circ$ ,  $22.11^\circ$ ,  $36.3^\circ$ ) and the olive pomace mill (at  $2\theta=26.9^\circ$ ,  $28.56^\circ$ ,  $28^\circ$ ) indicating a successful coating of silica over olive pomace.

### SEM and EDX analysis

The SEM is examined for the raw material of rice husk as seen in Fig. 5a–d. However, Fig. 5a shows the external shape

of the husk was covered with protuberances and hairs. The internal shape was smooth and with some porosities. The EDX spectra (Fig. 6a) showed that silicon is present in the rice husk with 21.64 wt%. While the raw material of pure olive pomace in Fig. 5b shows heterogeneous size distribution. Particle geometry is variable. Thus we observe the emergence of apparently well crystallized grains coexisting with fine powder clusters [5]. The EDX spectra in Fig. 6b for olive pomace showed that carbon is the most abundant element present in the olive pomace (45.63% weight) as, hemicelluloses and lipids are the main constituents of olive pomace. Table 2 illustrates EDX for the rice hull ash and olive Pomace. Figure 5c, extracted silica from rice husk is rough with appearing in some cavities. It shows also that, the silica agglomerates are jagged and irregular in shape and size [28] while Fig. 5d shows agglomerated semi-spherical particles of AM3 sample.

**TEM analysis** The obtained nano-silica powder is uniform and agglomerated in Fig. 7a, b. The shape of the silica

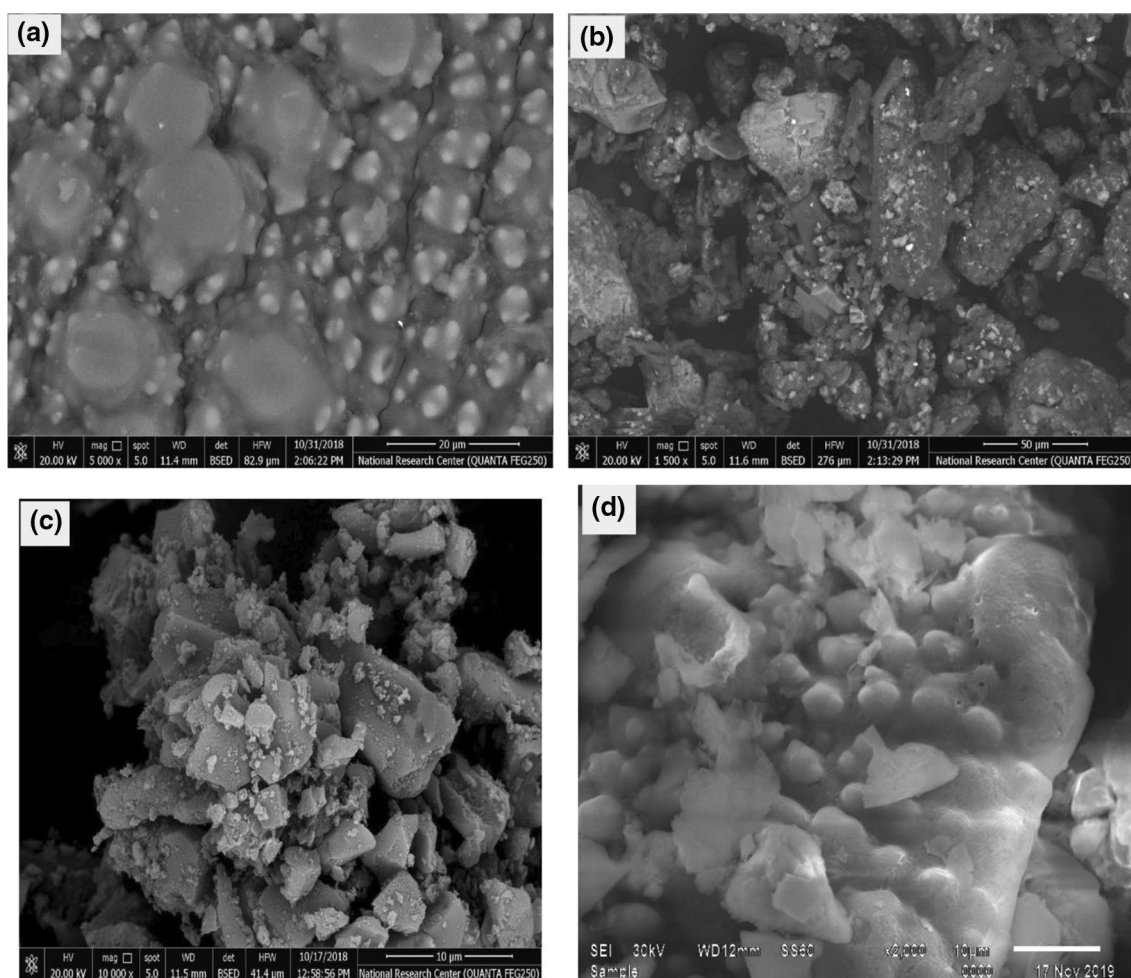


**Fig. 5** The SEM graphs of **a** rice husk mill, **b** olive pomace mill, **c** extracted silica, **d** AM3 nanocomposite

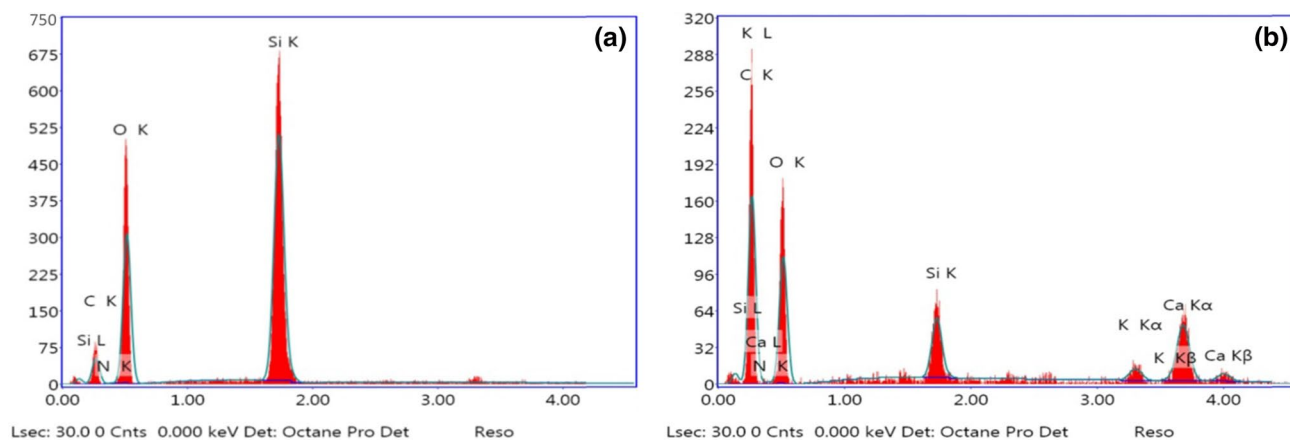


**Fig. 6** The EDX spectra of **a** rice husk mill, **b** olive pomace mill

**Table 2** The EDX of rice husk mill and olive pomace mill

Sample	Element	Weight%	Atomic%
Rice husk	C	24.86	33.42
	N	1.02	1.17
	O	52.48	52.97
	Si	21.64	12.44
Olive pomace	C	45.63	55.31
	N	2.04	2.12
	O	42.19	38.39
	Si	3.09	1.6
	K	1	0.37
	Ca	6.06	2.2

grains is spherical with an average homogeneous particle size distribution of about 10 nm, while the addition of 40% olive pomace to extracted silica in AM3 sample resulting in a small amount of aggregate spherical like particles of diameter size around 100 nm Fig. 7c, d.

### Thermal analysis

The thermogravimetric analysis can be observed in Fig. 8a–c. DTA displayed an endothermic peak at 70 °C for extracted silica Fig. 8a due to water evaporation. The TGA curve showed high thermal stability accompanied with tiny weight loss (~0.5%). Namely, this weight loss is attributed to the removal of moisture [28]. For olive pomace sample Fig. 8b, it has been stated that the thermal degradation characteristics of lignocellulosic materials are strongly influenced by their chemical composition (cellulose, hemicellulose, and lignin) [43]. Hemicellulose, cellulose, and lignin are chemically reactive and decompose thermochemically in the temperature range of 150–500 °C. So, olive pomace showed weight loss 58.8%. There are three exothermic peaks

at 81, 228, 423 °C due to evaporation of volatile and organic material degradation. The two endothermic peaks at 322, 481 °C attributed to decarbonation reaction [44]. For AM3 sample, Fig. 8c, two endothermic peaks at 92.7 and 351 °C due to hygroscopic water evaporation and decarbonation reaction respectively. The degradation of organic materials started from 246 to 518 °C. The total weight loss is 18.5%.

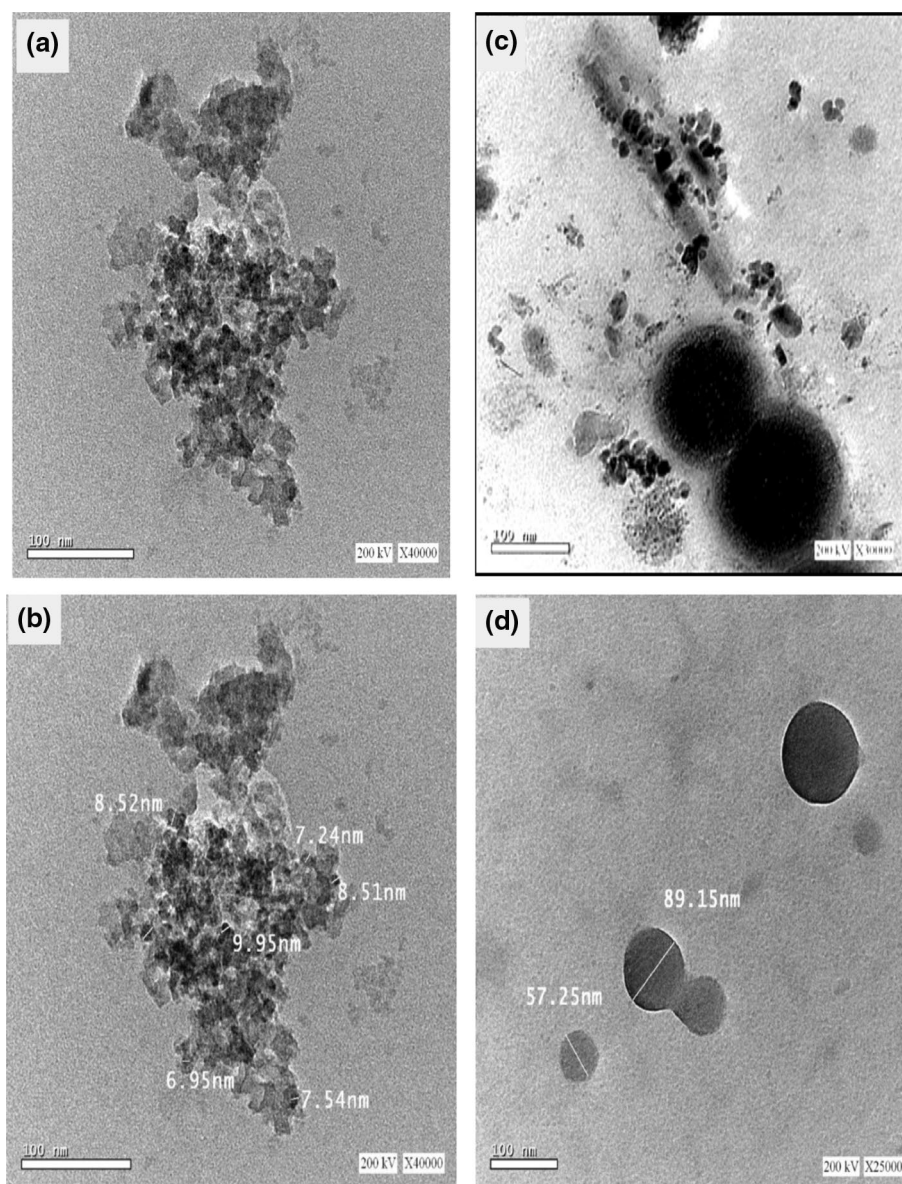
### Porosity measurements

The results in Table 3 show an increase in porosity percent for an extracted silica after adding 40% olive pomace from 35.62 to 44.64%. As the porosity increase, it was expected that the particle size will increase [45] confirming with TEM results. The bulk density estimates the volume of the sample plus the open and closed pores while the apparent density considers the volume of the samples and closed pores only. Comparing the densities for the samples, the bulk density of extracted silica sample is larger than AM3 sample. So, the volume of closed and open pores of extracted silica sample is smaller than that for AM3 nanocomposite sample. The introduction of open pores in AM3 nanocomposite will improve the adsorption capacity [46]. While the porosity of compact disc will decrease to 21.47%, the compaction caused ~23% decrease in the porosity of silica/olive pomace nanocomposite, the average pore diameter of Compacted disc-AM3 increases to ~three times the average pore diameter of AM3 nanocomposite.

### Sorption performance of the prepared nanocomposites

Initially, the synthesized nano-sized materials (AM1–CM9) were tested towards sorption some radionuclides ( $^{226}\text{Ra}$ ,  $^{210}\text{Po}$  and  $^{228}\text{Th}$ ) of the environmental in the TENORM-concentrate. The main characteristics of radionuclides chosen in

**Fig. 7** The TEM micrographs of **a, b** extracted silica, **c, d** AM3 nanocomposite



this study are summarized in Table 4. Moreover, the initial activity concentration of the studied alpha-emitters in the working solution was 685, 732 and 478 Bq/L for  $^{226}\text{Ra}$ ,  $^{210}\text{Po}$  and  $^{228}\text{Th}$  radionuclides, respectively. These values are high and above the permitted safe levels [47, 48].

#### Nano-sized material type (AM1-CM9)

The sorption efficiency (%) and distribution coefficients for the nanocomposite materials towards radionuclides of  $^{226}\text{Ra}$ ,  $^{210}\text{Po}$  and  $^{228}\text{Th}$  are given in Table 5. It is observed that sorption efficiencies (%) of all materials towards the radionuclides in 1M  $\text{HNO}_3$  solution take place the order  $^{226}\text{Ra} > ^{210}\text{Po} \gg ^{228}\text{Th}$ . However, the sorption efficiency by all material was within the ranges 58.4–89.4, 34.0–85.7 and 1.6–3.6% for radionuclides of  $^{226}\text{Ra}$ ,  $^{210}\text{Po}$  and  $^{228}\text{Th}$ ,

respectively. Also, the distribution coefficients had the same trend within ranges 281–1691, 104–1195 and 3.1–7.2 mL/g for  $^{226}\text{Ra}$ ,  $^{210}\text{Po}$  and  $^{228}\text{Th}$  radionuclides, respectively. Moreover, all materials showed fairly group sorption, especially for  $^{226}\text{Ra}$  and  $^{210}\text{Po}$ , while  $^{228}\text{Th}$  is not so. It is seen that the group sorption of  $^{226}\text{Ra}$  and  $^{210}\text{Po}$  was large by group A (AM1–AM3) nanocomposites.

#### Influence of acid solution type

To learn more knowledge about the sorption efficiency of the selected nanocomposite, i.e., AM3, sorption of the studied radionuclides has been investigated in different acid solutions included 1M nitric, sulfuric, perchloric and hydrochloric acid. The results were given in Table 6. It is found that the sorption efficiency (%) and distribution



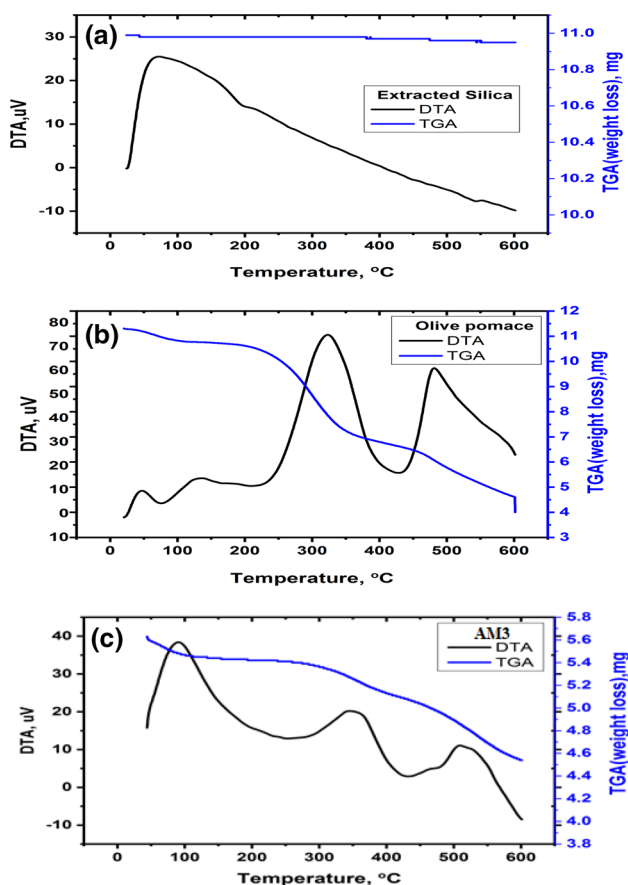


**Fig. 8** Thermal analysis of **a** extracted silica, **b** olive pomace, **c** AM3 nanocomposite

coefficients ( $K_d$ , mL/g) does not have certain behavior. This variation can be attributed to several factors as adsorbent nature, acid solution, ionic strength and/or species of the studied radionuclides [49–51]. As results, there are relatively high group sorption for  $^{226}\text{Ra}$  and  $^{210}\text{Po}$  than  $^{228}\text{Th}$

radionuclides by the AM3 (group A) in  $\text{HNO}_3$ ,  $\text{HClO}_4$  and  $\text{H}_2\text{SO}_4$ ; whereas the group sorption was highly observed for  $^{228}\text{Th}$  and  $^{226}\text{Ra}$  than  $^{210}\text{Po}$  in 1M HCl solution. However, the sorption was 93, 61 and 14% for  $^{228}\text{Th}$ ,  $^{226}\text{Ra}$  and  $^{210}\text{Po}$  radionuclides, respectively. Moreover, the high distribution coefficient was 1691 mL/g for  $^{226}\text{Ra}$ , 2580 mL/g for  $^{228}\text{Th}$  and 2954 mL/g for  $^{210}\text{Po}$  in 1M  $\text{HNO}_3$ , HCl and  $\text{HClO}_4$ , respectively, Table 6.

It seems that the variation in the results may depend largely on speciation of radionuclides in the acid solution. Therefore, some speciation diagrams are demonstrated to learn about the group sorption of radionuclides onto the nanocomposite AM3, Fig. 9a–e. The group sorption of  $\text{Ra}^{2+}$  with  $\text{Po}^{4+}$  or  $\text{Th}^{4+}$  species in 1M acid solutions (except  $\text{Ra}^{2+}$  with  $\text{H}_2\text{SO}_4$ ) may be due to interaction and/or ion-exchange processes of charged ions and/or complexes with the active moieties exist on the material surface. As seen in Fig. 9a, radium exists in all acid solutions (except with  $\text{H}_2\text{SO}_4$ ) as soluble positively charged ions like  $\text{Ra}^{2+}$ ,  $\text{RaNO}_3^+$  and  $\text{RaCl}^+$ ; while thorium appears as  $\text{Th}^{4+}$ ,  $\text{ThNO}_3^{3+}$ ,  $\text{ThCl}^{3+}$ ,  $\text{ThSO}_4^{2+}$  and  $\text{ThCl}_2^{2+}$ . In case of the sulfuric acid solution, sorption of  $\text{Ra}^{2+}$  is mainly attributed to its co-precipitation with the added carriers as  $\text{Ba}(\text{Ra})\text{SO}_4(\text{s})$  and/or  $\text{Pb}(\text{Ra})\text{SO}_4(\text{s})$  [52, 53]. Also, the low sorption of thorium is attributed to presence of  $^{228}\text{Th}$  soluble positive ion complexes in the both cases without interaction with material surface at the studied conditions [54].

On the other hand, polonium ( $\text{Po}^{4+}$ ) in all acid solution forms soluble salts and/or charged complexes with nitrates, acetates, chlorides, and other inorganic anions [49, 55–60]. At ~ 1M of mineral acid solutions (i.e., pH ~ 0), Po may exist as  $\text{Po}^{4+}$  [61, 62],  $\text{H}_3\text{PoO}_3^+$  [63, 64] and  $\text{H}_4\text{PoO}_3^{2+}$ . It was found that Po is a metastable between sparingly soluble species as  $(\text{PoO})_2(\text{SO}_4)_2 > \text{Po}(\text{SO}_4)_2 \cdot \text{H}_2\text{O}$  at ~ 1M sulfuric acid solution (Fig. 9b) and charged soluble species as  $\text{HPo}(\text{SO}_4)_3^- > \text{PoSO}_4^{2+}$  (Fig. 9c) [64, 65].

**Table 3** The porosity measurements for samples of silica, AM3 and compacted disc—AM3

Sorbent	Average pore diameter ( $\mu\text{m}$ )	Bulk density (g/mL)	Apparent density (g/mL)	Porosity (%)
Extracted silica	0.0548	0.5422	0.88422	35.62
AM3	0.2726	0.3808	0.6879	44.64
Compacted disc—AM3	0.610	0.4597	0.361	21.47

**Table 4** The main characteristic of  $^{226}\text{Ra}$ ,  $^{210}\text{Po}$  and  $^{228}\text{Th}$ -radionuclides [44]

Radionuclide	Half-life ( $t_{1/2}$ )	Decay mode	$E_\alpha$ (MeV)	$I_\alpha$ (%)	Main oxidation state	Initial activity (Bq/l)
$^{226}\text{Ra}$ (U-series)	1600 y	A	4.78	94.5	+2	685
$^{210}\text{Po}$ (U-series)	138 d	A	5.30	100.0	+4	723
$^{228}\text{Th}$ (Th-series)	1.91 y	A	5.42	72.7	+4	478

**Table 5** The sorption efficiency (%) and distribution coefficients ( $K_d$ ) of radionuclides found by the synthesized nanocomposite (AM1–CM9)

Material Code	Sorption efficiency (Mean $\pm$ SD) <sup>a</sup> (%)			Distribution coefficient ( $K_d$ , mL/g)		
	<sup>226</sup> Ra	<sup>210</sup> Po	<sup>228</sup> Th	<sup>226</sup> Ra	<sup>210</sup> Po	<sup>228</sup> Th
Group-A (AM1–AM3)						
AM1	87.9 $\pm$ 3.7	53.4 $\pm$ 2.2	2.2 $\pm$ 0.2	1446	229	4.5
AM2	89.4 $\pm$ 4.0	59.3 $\pm$ 3.0	2.5 $\pm$ 0.4	1691	292	5.2
AM3	<b>89.4 <math>\pm</math> 3.8</b>	62.3 $\pm$ 2.6	2.8 $\pm$ 0.2	<b>1691</b>	330	5.5
Group-B (BM4–BM6)						
BM4	<b>58.4 <math>\pm</math> 2.5</b>	<b>34.0 <math>\pm</math> 1.4</b>	<b>1.6 <math>\pm</math> 0.1</b>	<b>281</b>	<b>104</b>	<b>3.1</b>
BM5	65.0 $\pm$ 3.2	44.0 $\pm$ 3.1	1.8 $\pm$ 0.1	520	340	3.7
BM6	63.1 $\pm$ 2.7	42.0 $\pm$ 1.8	2.0 $\pm$ 0.1	342	143	4.2
Group-C (CM7–CM9)						
CM7	81.9 $\pm$ 3.4	<b>85.7 <math>\pm</math> 3.6</b>	3.0 $\pm$ 0.2	904	<b>1195</b>	6.2
CM8	82.8 $\pm$ 3.5	72.8 $\pm$ 3.1	3.2 $\pm$ 0.2	962	535	6.7
CM9	76.0 $\pm$ 3.2	78.7 $\pm$ 3.3	<b>3.4 <math>\pm</math> 0.2</b>	635	740	<b>7.2</b>

Minimum and maximum values are bolded

<sup>a</sup>Standard deviation ( $\pm$  SD)

**Table 6** The sorption efficiency (%) and distribution coefficients ( $K_d$ , mL/g) of <sup>226</sup>Ra, <sup>210</sup>Po and <sup>228</sup>Th by AM3 from different acid solutions (1M)

Radionuclide	Acid solution (1 mol/L)							
	HNO <sub>3</sub>		HCl		HClO <sub>4</sub>		H <sub>2</sub> SO <sub>4</sub>	
	%	$K_d$ (mL/g)	%	$K_d$ (mL/g)	%	$K_d$ (mL/g)	%	$K_d$ (mL/g)
<sup>226</sup> Ra	89.4 $\pm$ 4	<b>1691</b>	61.0 $\pm$ 3	<b>306</b>	37 $\pm$ 2	<b>118</b>	83 $\pm$ 4	<b>958</b>
<sup>210</sup> Po	62.3 $\pm$ 2.6	<b>330</b>	14.3 $\pm$ 1	<b>27</b>	94 $\pm$ 2	<b>2954</b>	38 $\pm$ 2	<b>121</b>
<sup>228</sup> Th	5.5 $\pm$ 0.2	<b>5.2</b>	93.0 $\pm$ 4	<b>2580</b>	5.5 $\pm$ 0.5	<b>11.6</b>	5.2 $\pm$ 0.4	<b>19.0</b>

In ~1M nitric or perchloric acid solution [63, 66, 67], polonium can be considered as a metastable between sparingly soluble nitrate complex, i.e., (PoO)<sub>2</sub>(NO<sub>3</sub>)<sub>3</sub>(OH) and soluble nitrate species as PoO(NO<sub>3</sub>)<sub>2</sub>-PoO(NO<sub>3</sub>)<sub>3</sub><sup>-</sup> > PoONO<sub>3</sub><sup>+</sup> at 25 °C, Fig. 9d. In 1M HCl solution, polonium exists as PoCl<sub>4</sub>(aq) > Po(OH)<sub>2</sub>Cl<sub>2</sub>(aq) ~ PoCl<sub>6</sub><sup>2-</sup> [63, 68], Fig. 9e.

The separation factors (SFs) have been calculated to know the possibility of the nanocomposite AM3 for selective separation of the radionuclides (<sup>226</sup>Ra, <sup>210</sup>Po and <sup>228</sup>Th) from the studied different acid solutions. The results are given in Table 7. It is clear that the high SF was ~325 between radionuclides of <sup>226</sup>Ra and <sup>228</sup>Th in 1M HNO<sub>3</sub> solution, and ~255 between <sup>210</sup>Po and <sup>228</sup>Th in 1M HClO<sub>4</sub> solution. As a result, the nanocomposite AM3 was selected to be utilized as ‘compact disc’ to examine its possibility to obtain a group separation or selective separation of radionuclides from 1M HNO<sub>3</sub> and HClO<sub>4</sub> solutions.

### Influence of nitric acid solution

Since the high sorption of <sup>226</sup>Ra radionuclides from the mixture was obtained by materials of group A and reached to

89% compared to 62% for <sup>210</sup>Po or 2.8% for <sup>228</sup>Th, the nanocomposite AM3 was selected to investigate the influence of nitric acid solution on sorption efficiency and the separation affinity of radionuclides. Thus, sorption of the studied radionuclides had been studied within the range 0.1–1M HNO<sub>3</sub>. The obtained results are represented in Fig. 10. It is seen that the change on the sorption behavior of <sup>226</sup>Ra-radionuclides onto AM3 was insignificant, i.e., 83–89%; while sorption of <sup>210</sup>Po or <sup>228</sup>Th-radionuclides decreased slightly. This means that sorption of Ra-isotopes does not influenced by H<sup>+</sup> ions competitions on the moieties in the adsorbent surface, whereas sorption of <sup>210</sup>Po or <sup>228</sup>Th radionuclides are slightly affected by H<sup>+</sup> ions competitions. Moreover, the group sorption of <sup>226</sup>Ra and <sup>210</sup>Po than <sup>228</sup>Th radionuclides was observed at 0.1M larger than 1M HNO<sub>3</sub>.

### Sorption efficiency by compact disc technique

In this technique, use of AM3 nanocomposite as ‘compact disc’ for separation of radionuclides has been done sequentially in 1M HNO<sub>3</sub> and HClO<sub>4</sub> solutions using a filtration system as demonstrated in Fig. 2. The radionuclides mixture was filtrated off through compact disc (Fig. 1a) with a flow

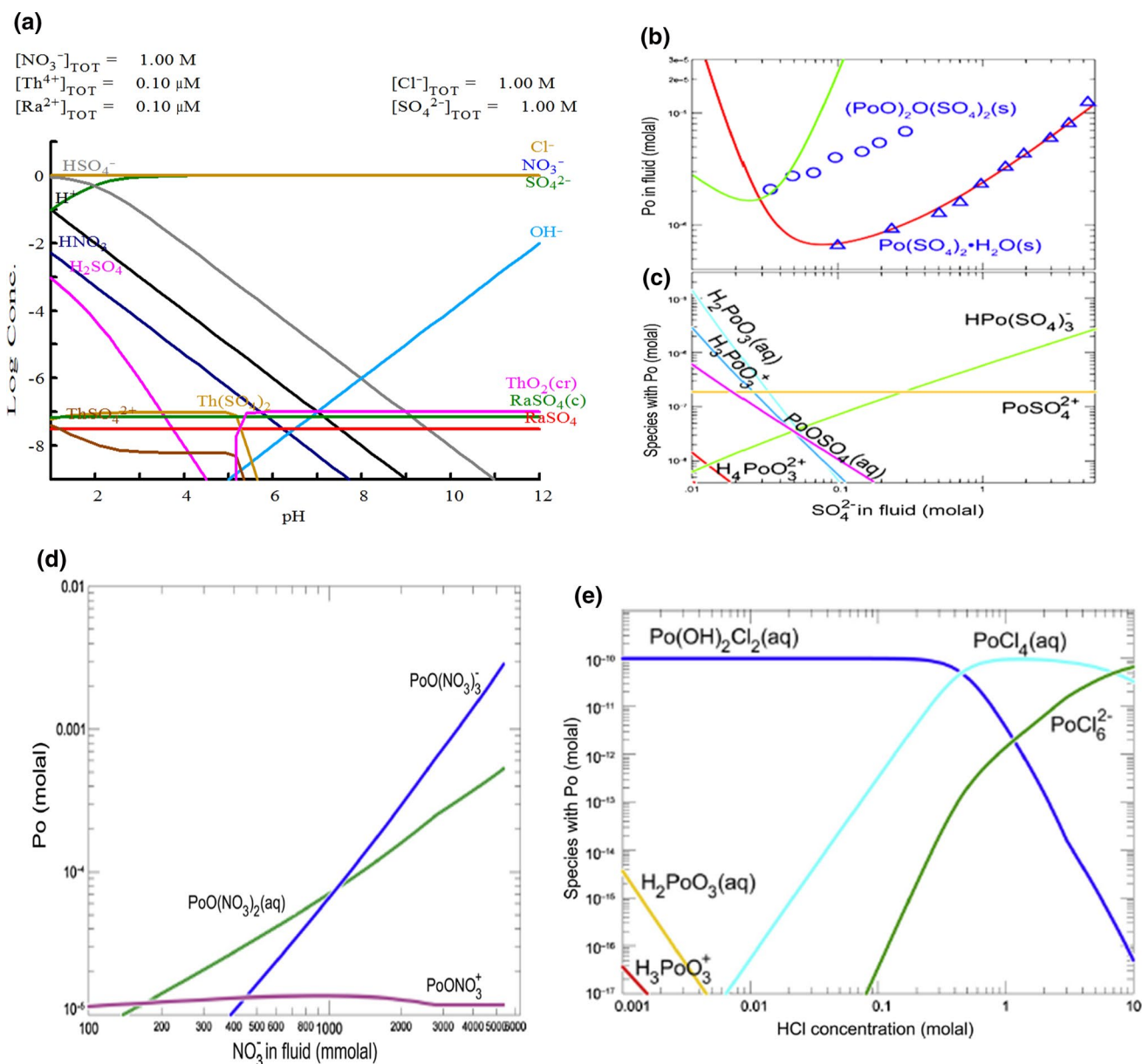


**Fig. 9** a Speciation diagram of  $Ra^{2+}$  and  $Th^{4+}$  in 1M  $HNO_3$ , HCl and  $H_2SO_4$  solutions. b, c Speciation diagram of  $Po^{+4}$  in sulfuric acid solution [60]. d Speciation diagram of  $Po^{+4}$  in nitric acid solution

[58, 61, 62]. e Speciation diagram diagram of  $Po^{+4}$  in hydrochloric acid solution [58, 63]

**Table 7** Separation factors (SF) of  $^{226}Ra$ ,  $^{210}Po$  and  $^{228}Th$  in 1M acid solutions by AM3

Radionuclide	SF			
	1M $HNO_3$	1M $H_2SO_4$	1M $HClO_4$	1M HCl
$^{226}Ra/^{210}Po$	5.8	7.9	0.04	11.4
$^{226}Ra/^{228}Th$	<b>325.3</b>	50.4	10.2	0.12
$^{210}Po/^{228}Th$	56.1	6.4	<b>254.6</b>	0.01

rate of ~0.6 mL/min under vacuum. The results are represented in Table 8.

When this technique carried out in 1M  $HNO_3$  solution,  $^{226}Ra$ ,  $^{210}Po$  and  $^{228}Th$ -radionuclides do not retained onto the compact disc, Fig. 11a. Therefore, the counts of all  $\alpha$ -emitters (i.e.,  $^{226}Ra$  at 4.78 MeV,  $^{210}Po$  at 5.31 MeV and  $^{228}Th$  at 5.42 MeV) in  $HNO_3$  solution are approximately the same before and after filtration through the compacted disc. In contrast, a significant difference in case of 1M  $HClO_4$  solution was observed for counts of the studied  $\alpha$ -emitters, Fig. 11b. The obtained sorption %

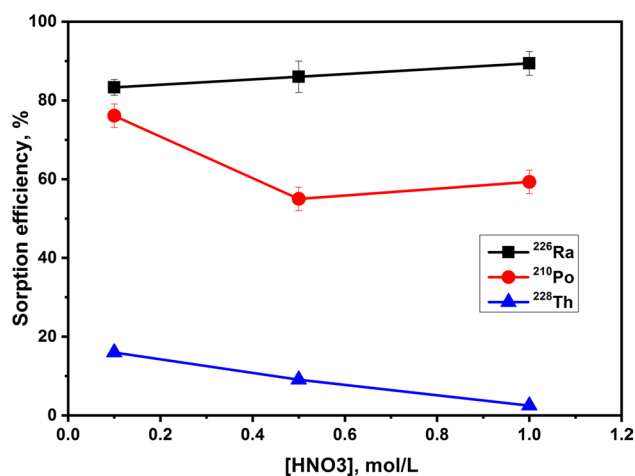


**Fig. 10** The influence of nitric acid solution on sorption behavior of <sup>226</sup>Ra, <sup>210</sup>Po and <sup>228</sup>Th radionuclides onto AM3

**Table 8** The sorption efficiency of <sup>226</sup>Ra, <sup>210</sup>Po and <sup>228</sup>Th radionuclides by compacted disc AM3

Radionuclide	Sorption efficiency (%)	
	1M HNO <sub>3</sub>	1M HClO <sub>4</sub>
<sup>226</sup> Ra	0.0	38.50 ± 2.4
<sup>210</sup> Po	0.0	77.00 ± 4.1
<sup>228</sup> Th	0.0	16.6 ± 1.2

by this technique reached to  $38.5 \pm 2.4$  and  $77.0 \pm 3.1\%$  for <sup>226</sup>Ra and <sup>210</sup>Po, respectively; whereas sorption of <sup>228</sup>Th was ~17%.

Figure 12 demonstrates a comparison between batch and compact disc for sorption of the radionuclides in 1M HClO<sub>4</sub> solution by the nanocomposite AM3. It noticed that the sorption of <sup>226</sup>Ra radionuclides was approximately the same (37.2–38.5%) by the both techniques. In case of <sup>210</sup>Po radionuclides, the sorption % was lowered to 77% by the compacted disc obtained by the batch technique (~94%). On contrast, sorption of <sup>228</sup>Th radionuclides increased to ~17% by the compact disc technique largely than that obtained by the batch technique (2.5%). These variations in the sorption

of the studied radionuclides by the both techniques may be attributed to the equilibration conditions, i.e., kinetic reasons and/or pore size parameter. It can be concluded that use of the nanocomposite materials (AM1–AM3) by batch or compacted disc techniques need more investigations to improve its group sorption of <sup>210</sup>Po and <sup>226</sup>Ra and/or selective separation of <sup>228</sup>Th-radionuclides from <sup>226</sup>Ra–<sup>210</sup>Po–<sup>228</sup>Th admixture. Thus, these materials can be considered as promising and efficient adsorbent to eliminate Ra-isotopes (<sup>228</sup>Ra, <sup>226</sup>Ra, <sup>224</sup>Ra, <sup>223</sup>Ra) and/or <sup>210</sup>Po in the effluents associated with strategic industries, like the front nuclear cycle operations to obtain the yellow cake, monazite processing and/or oil exploration.

## Conclusion

Nine nanocomposites (AM1–CM9) were prepared from local agriculture wastes (olive pomace and silica) and characterized by several physicochemical measurements (e.g., FTIR, XRD, SEM, EDX, TEM, TGA, DTA, porosity measurements). The sorption behavior of the nanocomposites was examined towards radionuclides of Ra, Po and Th in acid solution by batch and compacted disc techniques. It summarizes that the nanocomposites showed group sorption for <sup>226</sup>Ra (58–90%) and <sup>210</sup>Po (42–85%) radionuclides in 1M HNO<sub>3</sub>, while sorption of <sup>228</sup>Th does not exceed 7%. Thus, sorption efficiency nanocomposites cataloged into three groups A(M1–M3) > C(M7–M9) > B(M4–M6). Moreover, the sorption behavior was efficient in HNO<sub>3</sub> and HClO<sub>4</sub> compared with HCl or H<sub>2</sub>SO<sub>4</sub>. In the separation application by the ‘compacted disc’ as a novel technique, the nanocomposites AM-1–AM3 showed high group sorption for <sup>226</sup>Ra and <sup>210</sup>Po larger than <sup>228</sup>Th in HNO<sub>3</sub> and/or HClO<sub>4</sub>. Sorption of <sup>226</sup>Ra was similar to batch method, sorption of <sup>228</sup>Th increased slightly to ~17%, while sorption of <sup>210</sup>Po was decreased to 77%. Thus, use of the nanocomposite A (M1–M3) can be considered as promising and efficient nano-adsorbent for sorption of Ra-isotopes (e.g., <sup>228</sup>Ra, <sup>226</sup>Ra, <sup>224</sup>Ra, <sup>223</sup>Ra) and <sup>210</sup>Po-radionuclides from Ra–Po–Th radionuclides admixtures associated with some nuclear and industrial activities.

**Fig. 11** An alpha spectra for sorption of  $^{226}\text{Ra}$ ,  $^{210}\text{Po}$  and  $^{228}\text{Th}$ -radionuclides by AM3 compact disc in **a** 1M  $\text{HNO}_3$ , **b**  $\text{HClO}_4$

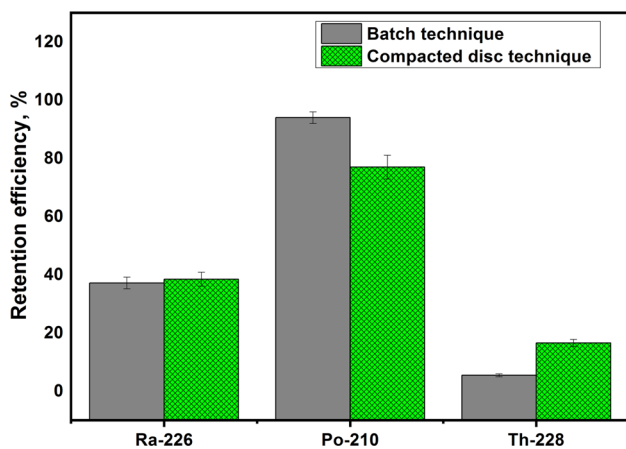
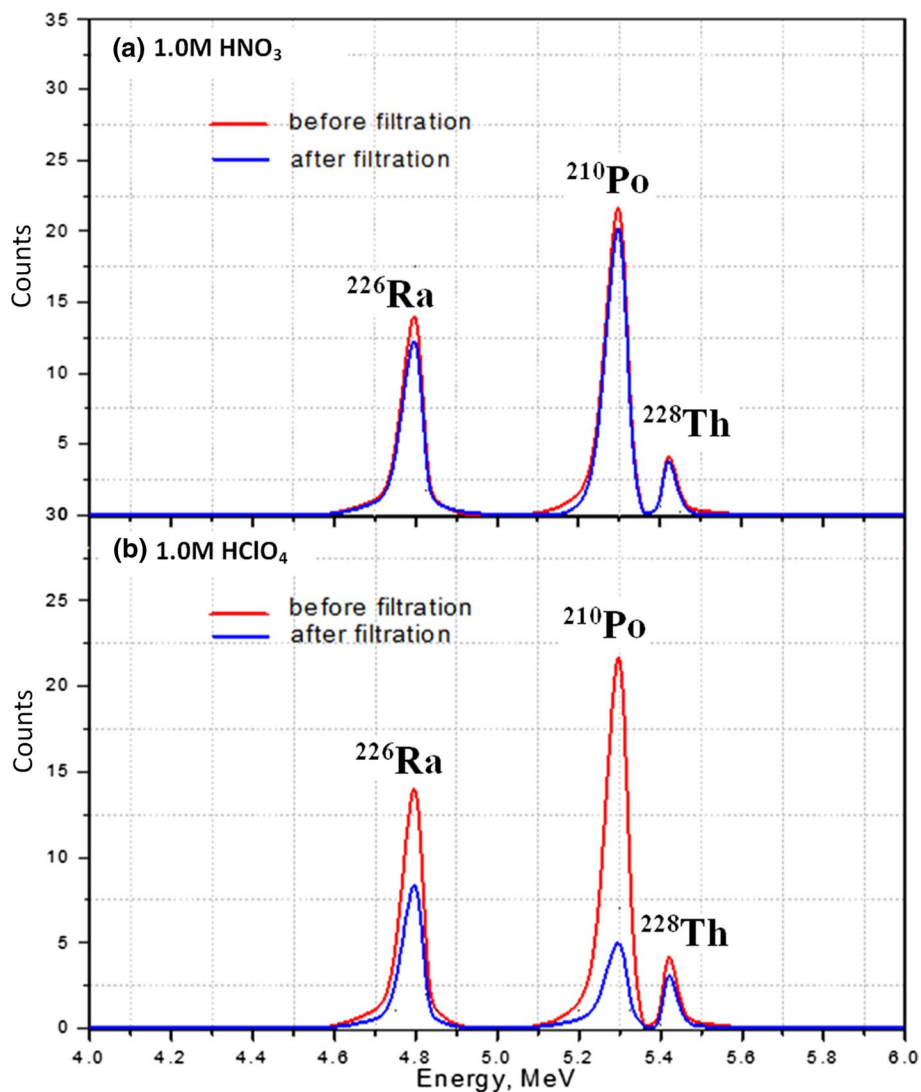


**Fig. 12** Histogram for sorption of  $^{226}\text{Ra}$ ,  $^{210}\text{Po}$  and  $^{228}\text{Th}$  radionuclides by 1M  $\text{HClO}_4$  using AM3 using batch and compacted disc techniques

## Compliance with ethical standards

**Conflict of interest** The authors declare that they have no conflict of interest.

## References

- Allan KF, El Afifi EM, Holial M (2017) Synthesis and application of poly(acrylamide–itaconic acid)/zirconium tungstate composite material for cesium removal from different solutions. Part Sci Technol 35(2):127–138. <https://doi.org/10.1080/02726351.2015.1131793>
- Khalil M, El-Aryan YF, El Afifi EM (2018) Sorption performance of light rare earth elements using zirconium titanate and polyacrylonitrile zirconium titanate ion exchangers. Part Sci Technol 36(5):618–627. <https://doi.org/10.1080/02726351.2017.1287141>

3. Yawen Y, Hua W, Deying X (2018) Applications of nanomaterials in nuclear waste management. *Multifunct Nanocompos Energy Environ Appl*. <https://doi.org/10.1002/9783527342501.ch18>
4. Soltani N, Bahrami A, Pech-Canul MI, González LA (2015) Review on the physicochemical treatments of rice husk for production of advanced materials. *Chem Eng J* 264:899–935. <https://doi.org/10.1016/j.cej.2014.11.056>
5. Iara J, Fernandes Daiane C, Felipe ALS, Alini LDC, Tatiana LACR, Carlos AMM, Vânia CS (2017) Characterization of silica produced from rice husk ash: comparison of purification and processing methods. *Mater Res* 20(Suppl 2):512–518. <https://doi.org/10.1590/1980-5373-MR-2016-1043>
6. Francesca P, Carolina CV, Luigi T (2010) Development of new composite biosorbents from olive pomace wastes. *Appl Surf Sci* 256:5492–5497. <https://doi.org/10.1016/j.apsusc.2009.12.146>
7. Zhang BJ, Davis SA, Mann S (2002) Starch gel templating of spongelike macroporous silicalite monoliths and mesoporous films. *Chem Mater* 14:1369–1375. <https://doi.org/10.1021/cm011251p>
8. Shen W, Li Z, Wang H, Liu Y, Guo Q, Zhang Y (2008) Photocatalytic degradation for methylene blue using zinc oxide prepared by codeposition and sol–gel methods. *J Hazard Mater* 152(1):172–175. <https://doi.org/10.1016/j.jhazmat.2007.06.082>
9. Attallah MF, Hilal MA, Mohamed YT (2018) Preliminary investigations on reducing the high radiation risk level of TENORM scale waste from petroleum industry. *Radiochim Acta* 106(9):793–800. <https://doi.org/10.1515/ract-2017-2904>
10. Attallah MF, El Afifi EM, Awwad NS, Aly HF (2013) Comparative study on the radioactivity of TE-NORM in different components of oil separator tank. *Radiochim Acta* 101:57–65. <https://doi.org/10.1524/ract.2013.1996>
11. Nath D (2018) Nanomaterial for the management of radioactive waste. In: Martínez L, Kharissova O, Kharisov B (eds) *Handbook of ecomaterials*. Springer, Cham. [https://doi.org/10.1007/978-3-319-48281-1\\_49-1](https://doi.org/10.1007/978-3-319-48281-1_49-1)
12. El Afifi EM, Khalil M, El-Aryan YF (2018) Leachability of radium-226 from industrial phosphogypsum waste using some simulated natural environmental solutions. *Environ Earth Sci* 77:94. <https://doi.org/10.1007/s12665-018-7277-x>
13. Tang YZ, Reeder RJ (2009) Uranyl and arsenate cosorption on aluminum oxide surface. *Geochim Cosmochim Acta* 73:2727–2743. <https://doi.org/10.1016/j.gca.2009.02.003>
14. Wang X, Zhang SW, Li JX, Xu JZ, Wang XK (2014) Fabrication of Fe/Fe<sub>3</sub>C@porous carbon sheets from biomass and their application for simultaneous reduction and adsorption of uranium(VI) from solution. *Inorg Chem Front* 1:641–648. <https://doi.org/10.1039/C4QI00071D>
15. Sun YB, Yang ST, Sheng GD, Guo ZQ, Tan XL, Xu JZ, Wang XK (2011) Comparison of U(VI) removal from contaminated groundwater by nanoporous alumina and non-nanoporous alumina. *Sep Purif Technol* 83:196–203. <https://doi.org/10.1016/j.seppur.2011.09.050>
16. Attallah MF, Elgazzar AH, Borai EH, El-Tabl AS (2016) Preparation and characterization of aluminum silicotitanate: ion exchange behavior for some lanthanides and iron. *J Chem Technol Biotechnol* 91:2243–2252. <https://doi.org/10.1002/jctb.4810>
17. Fan Q, Tanaka M, Tanaka K, Sakaguchi A, Takahashi Y (2014) An EXAFS study on the effects of natural organic matter and the expandability of clay minerals on cesium adsorption and mobility. *Geochim Cosmochim Acta* 135:49–65. <https://doi.org/10.1016/j.gca.2014.02.049>
18. Yang W, Zaoui A (2013) Behind adhesion of uranyl onto montmorillonite surface: a molecular dynamics study. *J Hazard Mater* 261:224–234. <https://doi.org/10.1016/j.jhazmat.2013.07.021>
19. Verma PK, Pathak PN, Mohapatra PK, Godbole SV, Kadam RM, Veligzhanin AA, Zubavichus YV, Kalmykov SN (2014) Influences of different environmental parameters on the sorption of trivalent metal ions on bentonite: batch sorption, fluorescence, EXAFS and EPR studies. *Environ Sci Process Impacts* 16: 904–915. <https://doi.org/10.1039/C3EM00563A>
20. Kerisit S, Liu CX (2014) Molecular dynamics simulations of uranyl and uranyl carbonate adsorption at aluminosilicate surfaces. *Environ Sci Technol* 48:3899–3907. <https://doi.org/10.1021/es405387c>
21. Choung S, Kim M, Yang JS, Kim MG, Um W (2014) Effects of radiation and temperature on iodide sorption by surfactant-modified bentonite. *Environ Sci Technol* 48:9684–9691. <https://doi.org/10.1021/es501661zn>
22. Wang ZM, Zachara JM, Shang JY, Jeon C, Liu J, Liu CX (2014) Investigation of U(VI) adsorption in quartz-chlorite mineral mixtures environ. *Sci Technol* 48:7766–7773. <https://doi.org/10.1021/es500537g>
23. Li XL, Mu WJ, Xie X, Liu BJ, Tang H, Zhou GH, Wei HY, Jian Y, Luo SZ (2014) Strontium adsorption on tantalum-doped hexagonal tungsten oxide. *J Hazard Mater* 264:386–394. <https://doi.org/10.1016/j.jhazmat.2013.11.032>
24. Song WC, Liu MC, Hu R, Tan XL, Li JX (2014) Water-soluble polyacrylamide coated-Fe<sub>3</sub>O<sub>4</sub> magnetic composites for high-efficient enrichment of U(VI) from radioactive waste. *Chem Eng J* 246:268–276. <https://doi.org/10.1016/j.cej.2014.02.101>
25. Borai E, Attallah M, Koivula R, Paajanen A, Harjula R (2012) Separation of Europium from cobalt using antimony silicates in sulfate acidic media. *Min Process Extr Metall Rev* 33:204–219. <https://doi.org/10.1080/08827508.2011.562951>
26. Rizk HE, Attallah MF, Ali AMI (2017) Investigations on sorption performance of some radionuclides, heavy metals and lanthanides using mesoporous adsorbent material. *J Radioanal Nucl Chem* 314:2475–2487. <https://doi.org/10.1007/s10967-017-5620-4>
27. Yu S, Wang X, Yang S et al (2017) Interaction of radionuclides with natural and manmade materials using XAFS technique. *Sci China Chem* 60:170–187. <https://doi.org/10.1007/s11426-016-0317-3>
28. Dakroury GA, Abo-Zahra ShF, Hassan HS, Nady AF (2020) Utilization of silica-chitosan nanocomposite for removal of <sup>152+154</sup>Eu radionuclide from aqueous solutions. *J Radioanal Nucl Chem* 322(3):439–455. <https://doi.org/10.1007/s10967-019-06951-6>
29. El Afifi EM, Attallah MF, Borai EH (2016) Utilization of natural hematite as reactive barrier for immobilization of radionuclides from radioactive liquid waste. *J Environ Radioact* 151(Part 1):156–165. <http://dx.doi.org/10.1016/j.jenvrad.2015.10.001>
30. El Afifi EM, Borai EH (2006) Performance characteristics of sequential separation and quantification of lead-210 and polonium-210 by ion exchange chromatography and nuclear spectrometric measurements. *J Environ Qual* 35(2):568–574. <https://doi.org/10.2134/jeq2005.0223>
31. Vasileva P (2016) Synthesis and characterization of ZnO nanocrystals in starch matrix. In: *Scientific proceedings II international scientific conference, material science non equilibrium phase transformations*. ISSN 1310-3946
32. Attallah MF, Hamed Mostafa M, El Afifi EM (2019) Remediation of TENORM scale waste generated from petroleum industry using single and mixed micelles solutions. *J Mol Liq* 294:111565. <https://doi.org/10.1016/j.molliq.2019.111565>
33. Warren CJ, Xing B, Duds MJ (1990) Simple microwave digestion technique for elemental analysis of mineral soil samples. *Can J Soil Sci* 70:617–620
34. Twyman RM (2005) Sample dissolution for elemental analysis: wet digestion. In: Worsfold P, Townshend A, Poole C (eds) *Encyclopedia of analytical science*, vol 8, 2nd edn. Elsevier Science, London, pp 146–153
35. Attallah MF, Rizk SE, El Afifi EM (2018) Efficient removal of iodine and chromium as anionic species from radioactive

- liquid waste using prepared iron oxide nanofibers. *J Radioanal Nucl Chem* 317(2):933–945. <https://doi.org/10.1007/s10967-018-5938-6>
36. Wang M, Zagorodny A, Muhammed M (2015) HYDRA-MEDUSA software: hydrochemical equilibrium constant database. Ignasi Puigdomened Inorganic Chemistry, Royal Institute of Technology, 10044 Stockholm, Sweden
  37. Yuvakkumar R, Elango V, Rajendran V, Kannan N (2014) High-purity nano silica powder from rice husk using a simple chemical method. *J Exp Nanosci* 9(3):272–281. <https://doi.org/10.1080/17458080.2012.656709>
  38. Thanh NT, Thi VAP, My LPL, Thi PTN, Van MT (2013) Synthesis of amorphous silica and sulfonic acid functionalized silica used as reinforced phase for polymer electrolyte membrane. *Adv Nat Sci Nanosci Nanotechnol* 4(4):6. <https://doi.org/10.1088/2043-6262/4/4/045007>
  39. Lamia MH, Farid Z, Sonia MA, Mouloud K (2018) Olive Pomace: from an Olive mill waste to resource, an overview of the new treatments. *J Crit Rev* 5(6):6. <https://doi.org/10.22159/jcr.2018v5i5.28840>
  40. Babakhouya N, Abdouni M, Louhab K (2018) Preparation and characterization study of an olive pomace—polyaniline composite conductor in the recovery of heavy metals by electrosorption and adsorption. *Alger J Environ Sci Technol* 4(2):720–727
  41. Jan-Jezreel FS, Rizalinda LL, Kamolwan R, Sanchai P, Jatuporn W (2011) Properties of silica from rice husk and rice husk ash and their utilization for zeolite  $\gamma$  synthesis. *Quim. Nova* 34(8):1394–1397. <https://doi.org/10.1590/S0100-40422011000800018>
  42. International Centre for Diffraction Data (2007) Powder diffraction files
  43. Garcia-Ibanez P, Sanchez M, Cabanillas A (2006) Thermogravimetric analysis of olive-oil residue in air atmosphere. *Fuel Process Technol* 87(2):103–107. <https://doi.org/10.1016/j.fuproc.2005.08.005>
  44. Eliche-Quesada D, Felipe-Sesé MA, Infantes-Molina A (2016) Olive stone ash as secondary raw material for fired clay bricks. *Adv Mater Sci Eng* 2016:9
  45. Fisenne IM (1997) Radionuclide data, section 5, Vol. 1, HASL-300, 28th Edition, Environmental Measurements Laboratory. US Department of Energy, New York
  46. Shuo Z (2017), Relation between particle size distribution and porosity in Dump leaching. MSc thesis in the faculty of graduate and postdoctoral studies the university of British Columbia. <https://doi.org/10.14288/1.0357233>
  47. WHO (2011) Guidelines for drinking-water quality, 4th edn. WHO Publications, Geneva
  48. IAEA (2016) Criteria for radionuclide activity concentrations for food and drinking water (IAEA-TECDOC-1788)
  49. Lehto J, Hou X (2011) Chemistry and analysis of radionuclides: laboratory techniques and methodologies. WILEY-VCH Verlag & Co. KGaA, Boschstr, Weinheim
  50. Porcelli D, Kim CH-K, Martin P, Moore WS, Phaneuf M (2014) Properties of radium. In: The environmental behavior of radium, Revised Edition, Technical Reports Series No. 476, Published in 24 March 2014 by the IAEA, Vienna, Chap 2, pp 6–32
  51. Aurian A, Phaneuf MO, Mabit L (2015) Mobility and bioavailability of radionuclides in soils. In: Walther C, Gupta DK (eds) Radionuclides in the environment. Springer, Cham, Chap 2, pp 37–59
  52. El Afifi EM, Borai EH, Shahr El-Din AM (2019) New approaches for efficient removal of some radionuclides and iron from rare earth liquor of monazite processing. *Int J Environ Sci Technol* 16(12):7735–7746. <https://doi.org/10.1007/s13762-018-02183-5>
  53. Bori EH, ElAfifi EM, Shahr El-Din AM (2017) Selective elimination of natural radionuclides during the processing of high grade monazite concentrates by caustic conversion method. *Korean J Chem Eng* 34(4):1091–1099. <https://doi.org/10.1007/s11814-016-0350-9>
  54. Hyde EK (1960) The radiochemistry of thorium. National Academy of Sciences—National Research Council, Nuclear Science Series (NAS—NS 3004). US Atomic Energy Commission, USA
  55. Figgins PE (1961) The radiochemistry of polonium. National Academy of Sciences—National Research Council, Nuclear Science Series (NAS—NS 3037). US Atomic Energy Commission, USA
  56. Thakur P, Ward AL (2019)  $^{210}\text{Po}$  in the environment: insight into the naturally occurring polonium isotope. *J Radioanal Nucl Chem*. <https://doi.org/10.1007/s10967-019-06939-2>
  57. Carvalho F, Fernandes S, Fesenko S, Holm E, Howard B, Martin P, Phaneuf M, Porcelli D, Prohl G, J. Twining (2017) The environmental behaviour of polonium, chapter 3: properties of polonium. Technical report series No. 484, Publishing Section, International Atomic Energy Agency (IAEA), Vienna, pp 15–33
  58. Suganuma H, Hataye I (1981) Solvent extraction study on the hydrolysis of tracer concentration of Po(IV) in chloride solution. *J Inorg Nucl Chem* 43(10):2511–2515. [https://doi.org/10.1016/0022-1902\(81\)80292-8](https://doi.org/10.1016/0022-1902(81)80292-8)
  59. Hataye I, Suganuma H, Sakata M (1981) Solvent extraction study on the hydrolysis of tracer concentration of polonium(IV) in nitrate solutions. *J Inorg Nucl Chem* 43:2575–2577. [https://doi.org/10.1016/0022-1902\(81\)80309-0](https://doi.org/10.1016/0022-1902(81)80309-0)
  60. Koch VH, Schmidt H (1963) The determination of the hydrolysis constants in aqueous solutions after the ion exchange method. Part B *Chem Biochem Biophys Biol Relat* 1963:936–941
  61. Starik IE, Ampelogova N, Kuznetsov B (1964) Complex formation of polonium with the chloride ion in aqueous and aqueous-acetone solutions. *Radiokhim* 6:507–509
  62. Katzlberger C (2000), Speciation, analysis and ion-exchange behavior of polonium and other natural radionuclides in drinking water. PhD thesis. Universität Wein
  63. Ram R, Vaughan J, Etschmann B, Brugger J (2019) The aqueous chemistry of polonium(Po) in environmental and anthropogenic processes: review. *J Hazard Mater* 380:120725. <https://doi.org/10.1016/j.jhazmat.2019.06.002>
  64. Brown SA (2001), The aqueous chemistry of polonium and its relationship to mineral processing streams. University of Western Sydney
  65. Bagnall KW, Freeman JH (1956) The sulphates and selenate of polonium. *J Chem Soc* 878:4579–4582. <https://doi.org/10.1039/JR9560004579>
  66. Ampelogova N (1973) Investigation of complex formation of Polonium by an exchange method. *Radiokhim* 15:813–820
  67. Orban E (1954) The solubility of polonium nitrate in nitric acid solutions. Mound Lab, Miamisburg
  68. Younes A (2013) Exploration de la chimie du polonium. PhD thesis. Université de Nantes

**Publisher's Note** Springer Nature remains neutral with regard to jurisdictional claims in published maps and institutional affiliations.